

Renormalization group flow of quartic perturbations in graphene: Strong coupling and large- N limits

Joaquín E. Drut and Dam Thanh Son

Institute for Nuclear Theory, University of Washington, Seattle, Washington 98195-1550, USA

(Received 12 October 2007; published 15 February 2008)

We explore the renormalization group flow of quartic perturbations in the low-energy theory of graphene, in the strong Coulomb coupling and large- N limits, where N is the number of fermion flavors. We compute the anomalous dimensions of the quartic couplings u up to leading order in $1/N$ and find both relevant and irrelevant directions in the space of quartic couplings. We discuss possible phase diagrams and relevance for the physics of graphene.

DOI: [10.1103/PhysRevB.77.075115](https://doi.org/10.1103/PhysRevB.77.075115)

PACS number(s): 73.63.Bd, 05.10.Cc

I. INTRODUCTION

Graphene, a single layer of graphite, has lately attracted increasing attention, especially since its experimental realization.¹ This material presents a number of unusual electronic features, such as a Landau level structure that gives rise to half-integer quantum Hall effect. In general, those properties can be traced back to the low-energy spectrum, governed by two-component massless fermions that come in four flavors: two due to electronic spin and two from degenerate Dirac points in the band structure.² The quasirelativistic electronic spectrum is characterized by a velocity $v \approx c/300 \ll c$, where c is the speed of light. However, the Coulomb interaction, which is instantaneous for all practical purposes, breaks this emergent Lorentz invariance. In particular, the electron velocity becomes scale dependent.³

It was noted recently⁴ that a generalization of the low-energy theory that describes graphene possesses a quantum critical point. Reference 4 considered a model of N species of $2+1$ dimensional two-component massless Dirac fermions interacting through a three-dimensional instantaneous Coulomb interaction with a coupling constant g . It was then shown, by analyzing the renormalization group (RG) flow of the fermion velocity, that for sufficiently large N , the strongly coupled limit $g^2 N/v \rightarrow \infty$ is a quantum critical point, characterized by a dynamic critical exponent $z = 1 - 8/(\pi^2 N) + O(1/N^2)$. It was also argued that real graphene is close to this critical point for a large momentum window.

In the present work, we further explore the quantum critical properties of this theory by studying the RG flow of various quartic perturbations of the varieties of Thirring⁵ and Gross and Neveu.⁶ These four-fermion interactions are irrelevant at weak coupling but obtain nontrivial anomalous dimensions of order $1/N$ at the strong coupling fixed point. If a four-Fermi coupling becomes relevant below some N , one may expect dynamical gap generation, in which case the system becomes an insulator or that the system would flow to another fixed point.

The question of whether the Coulomb interaction makes graphene an insulator has been considered previously. In Ref. 7, it was found from solving the gap equation with a screened Coulomb interaction that, for $N < 8/\pi \approx 2.55$, a gap opens at sufficiently large coupling. For $N > 8/\pi$, the system

remains gapless at all couplings. This was confirmed in Ref. 8 using a similar approach. However, as the approximations employed in these works are uncontrolled, one would like to explore alternative approaches to this problem. The RG analysis in this paper is one of them. (Instability toward ferromagnetism has also been considered.⁹)

We implement a Wilson-Fisher RG transformation and find the anomalous dimensions of the various couplings. Throughout the paper, the Coulomb parameter $\lambda = g^2 N/32v$ is kept finite and the limit $\lambda \rightarrow \infty$ is discussed at the end. In this limit, we identify both relevant and irrelevant directions in the parameter space of the quartic couplings and discuss possible scenarios, including gap generation and the flow to a non-Gaussian fixed point. At the end of our results in Sec. IV, we address the relevance of our findings for real graphene.

The paper is organized as follows: the model and Feynman rules are presented in Sec. II, the details of the calculation are outlined in Sec. III, the results are discussed in Sec. IV, and the conclusions presented in Sec. V.

II. MODEL AND FEYNMAN RULES

Consider a model of $N/2$ flavors of four-component relativistic fermions (or N flavors of two-component fermions) ψ_a interacting through an instantaneous Coulomb interaction and through generic $U(N/2)$ -symmetric quartic interactions. The corresponding Euclidean action is

$$\begin{aligned}
 S_E = & - \int dt d^2x (\bar{\psi}_a \gamma^0 \partial_0 \psi_a + v \bar{\psi}_a \gamma^i \partial_i \psi_a + i A_0 \bar{\psi}_a \gamma^0 \psi_a) \\
 & + \frac{1}{2g^2} \int dt d^3x (\partial_i A_0)^2 + \frac{1}{2N} \int dt d^2x [u_1 (\bar{\psi}_a \psi_a)^2 \\
 & + u_2 (\bar{\psi}_a \gamma_0 \psi_a)^2 + u_3 (\bar{\psi}_a \gamma_0 \gamma_5 \psi_a)^2 + u_4 (\bar{\psi}_a \gamma_0 \psi_a)^2 \\
 & + u_5 (\bar{\psi}_a \gamma_i \psi_a)^2 + u_6 (\bar{\psi}_a \gamma_5 \psi_a)^2], \quad (2.1)
 \end{aligned}$$

where the γ^μ , $\mu=0,1,2$ (we shall also use Latin indices for the spatial directions) are Dirac matrices satisfying a Euclidean Clifford algebra $\{\gamma^\mu, \gamma^\nu\} = 2\delta^{\mu\nu}$, and $\gamma^5 = \gamma^0 \gamma^1 \gamma^2$. We can choose, for example, a representation of this algebra in which

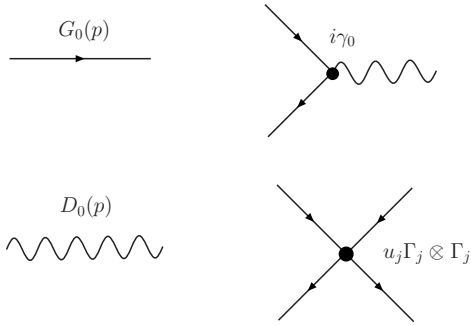


FIG. 1. Feynman rules (see text for details).

$$\gamma^0 = \begin{pmatrix} \sigma^3 & 0 \\ 0 & -\sigma^3 \end{pmatrix}, \quad \gamma^j = \begin{pmatrix} \sigma^j & 0 \\ 0 & -\sigma^j \end{pmatrix}, \quad (2.2)$$

where σ^j are the Pauli matrices. In the real world, $N/2=2$, corresponding to two spin polarizations of the electrons. The two two-component spinors near the two valleys are combined into a four-component spinor. The action [Eq. (2.1)] is invariant under spin rotations, but it is not invariant under rotations in the valley space. (The two degenerate Dirac points in the band structure of graphene are sometimes referred to as valleys. Thus, rotations in valley space correspond to operations that mix the upper and lower components of the four-component Dirac fermions of our theory.) Notice that the four-Fermi terms are rotationally invariant, but not Lorentz invariant: the latter is broken by the Coulomb interaction. Apart from the four-Fermi terms written in Eq. (2.1), one can also introduce an independent set equal to γ^3 times the vertices already included, where γ^3 is linearly independent from the other γ matrices and $\{\gamma^3, \gamma^\mu\}=0$. One possible choice is

$$\gamma^3 = \begin{pmatrix} 0 & 1 \\ 1 & 0 \end{pmatrix}. \quad (2.3)$$

Such matrices, together with the ones already considered, form a complete basis for the algebra of 4×4 Dirac matrices. We restrict for the moment to the action [Eq. (2.1)], but we shall comment on these extra vertices in Sec. IV.

We shall use the large- N limit to do calculations at large values of the coupling g , so N will remain arbitrary (but large) until the end. Notice that, unlike the fermionic degrees of freedom, the Coulomb field A_0 lives in 3+1 dimensions, which is reflected in its kinetic term. In the strong coupling $g \rightarrow \infty$ limit, this term disappears and the A_0 propagator is dominated by quantum corrections coming from the fermion loops, as we shall see below.

In 2+1 dimensions, the naive dimensions of the fields and couplings are as follows: $[\psi]=m$, $[A_0]=m$, $[g]=m^0$, and $[u_j]=m^{-1}$.

The Feynman rules are as in Fig. 1, where the fermion propagator is

$$D(p) = \text{wavy line} + \text{wavy line with fermion loop} + \text{wavy line with two fermion loops} + \dots$$

FIG. 2. Resummation of the one-loop self-energy contribution to the boson propagator.

$$G_0(p) = \frac{i\not{p}}{p^2}, \quad (2.4)$$

where $p=(p_0, \vec{p})$, \vec{p} being a two-dimensional momentum vector. Here and in the rest of the paper, we use the notation $p = \gamma^0 p_0 + \nu \vec{\gamma} \cdot \vec{p}$ and $p^2 = p_0^2 + \nu^2 |\vec{p}|^2$. The boson-fermion interaction vertex is $i\gamma_0$, and the quartic vertices are $-\frac{u_j}{N} \Gamma_j \otimes \Gamma_j$, with $\Gamma_j \in \{1, \gamma_0 \gamma_i, \gamma_0 \gamma_5, \gamma_0, \gamma_i, \gamma_5\}$.

Finally, the bare boson (A_0) propagator is

$$D_0(p) = \frac{g^2}{2|\vec{p}|}. \quad (2.5)$$

In the large N , finite $g^2 N$ limit, we must resum the fermion loop contributions to this propagator (see Fig. 2).

Such resummation (which is equivalent to the random phase approximation) results in a dressed boson propagator that we shall use in the rest of this work, as shown in Figs. 2 and 3,

$$\begin{aligned} D(q) &= \left(\frac{2|\vec{q}|}{g^2} + \frac{N|\vec{q}|^2}{16\sqrt{q^2}} \right)^{-1} \\ &= \frac{16\sqrt{q^2}}{N|\vec{q}|^2} \left(1 + \frac{1}{\lambda} \frac{\sqrt{q^2}}{|\vec{q}|} \right)^{-1} \\ &= \frac{g^2}{2|\vec{q}|} \left(1 + \lambda \frac{|\vec{q}|}{\sqrt{q^2}} \right)^{-1}, \end{aligned} \quad (2.6)$$

where $\lambda = g^2 N / (32\nu)$.

III. CALCULATION OF THE RENORMALIZATION GROUP FLOW

We implement a Wilsonian RG procedure whereby we integrate out the modes in the momentum shell $\Lambda_1 < p < \Lambda_0$ and then rescale the coordinates as well as the fields. The RG equation has the form

$$\frac{\partial \mathbf{u}(p)}{\partial \ln p} = [1 - \mathbf{M}(\lambda)] \mathbf{u}(p), \quad (3.1)$$

where $[\mathbf{u}]_i = u_i$ and $\mathbf{M}(\lambda)$ is a 6×6 matrix. The 1 in the right-hand side comes from the naive dimension of u_i . Furthermore,

FIG. 3. One-loop self-energy contribution to the boson propagator.

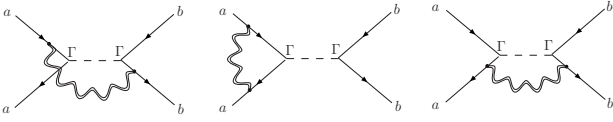


FIG. 4. Contributions to the RG flow of u_j coming from vertex renormalization. a and b are flavor indices and Γ is a generic four-Fermi vertex. The dashed line is intended to show the difference between the loops in the various diagrams. Exchange of dummy indices leads to the same diagrams and results in an overall factor of 2.

$$\mathbf{M}(\lambda) = \mathbf{M}_v(\lambda) + \mathbf{M}_{wf}(\lambda), \quad (3.2)$$

where \mathbf{M}_v comes from the vertex corrections and \mathbf{M}_{wf} comes from wave function renormalization.

A. Vertex renormalization

To the first nontrivial order in $1/N$, finding the RG flow of u_j entails computing the diagrams in Fig. 4 using the Feynman rules described in the previous section.

The loop integrals have the same form for all three diagrams, namely,

$$\begin{aligned} & \frac{16}{N} \int_{\Lambda_1}^{\Lambda_0} \frac{d^3q}{(2\pi)^3} \frac{q^\mu q^\nu \lambda}{q^4 |\vec{q}|} \left(1 + \lambda \frac{|\vec{q}|}{\sqrt{q^2}}\right)^{-1} \\ &= \frac{4}{N\pi^2} \ln \left[\frac{\Lambda_0}{\Lambda_1} \right] \begin{cases} I_0(\lambda) & \text{for } \mu = \nu = 0 \\ \frac{I_1(\lambda)}{2} & \text{for } \mu = \nu = i, \end{cases} \end{aligned} \quad (3.3)$$

and vanish for $\mu \neq \nu$. The integration region is spherically symmetric. Furthermore, notice that the integrand is independent of the azimuthal angle and that the remaining radial and angular integrals are decoupled because $|\vec{q}| = \sqrt{q^2} \sqrt{1-t^2}$, where $t = \cos \theta$ and θ is the polar angle, making the calculation straightforward. We have used the following definitions:

$$\begin{aligned} I_0(\lambda) &= \int_{-1}^1 dt \frac{t^2}{\sqrt{1-t^2}} \frac{\lambda}{1 + \lambda \sqrt{1-t^2}} \\ &= -2 + \frac{\pi}{\lambda} + \frac{2\sqrt{\lambda^2-1}}{\lambda} \ln[\lambda + \sqrt{\lambda^2-1}], \end{aligned} \quad (3.4)$$

$$\begin{aligned} I_1(\lambda) &= \int_{-1}^1 dt \frac{\lambda \sqrt{1-t^2}}{1 + \lambda \sqrt{1-t^2}} \\ &= 2 - \frac{\pi}{\lambda} + \frac{2}{\lambda \sqrt{\lambda^2-1}} \ln[\lambda + \sqrt{\lambda^2-1}]. \end{aligned} \quad (3.5)$$

In the large λ limit, $\lambda \rightarrow \infty$,

$$I_0(\lambda) \rightarrow -2 + 2 \ln[\lambda + \sqrt{\lambda^2-1}], \quad (3.6)$$

while

$$I_1(\lambda) \rightarrow 2. \quad (3.7)$$

The divergence of $I_0(\lambda \rightarrow \infty)$ is associated with the fact that the Coulomb interaction is unscreened at zero momentum

and nonzero frequency. As we shall see, however, all such divergences cancel out in the β functions for u_i .

With the above identities at hand, it is not very difficult to compute the contributions of the diagrams in Fig. 4 to the β functions. The only significant step that remains to be discussed is straightforward Dirac algebra to find the products of a small number of γ matrices (coming from the vertices and the fermion propagators). For instance, for $\Gamma_4 = \gamma_0$, the calculation of the diagram in the middle of Fig. 4 entails computing

$$\gamma_0 \gamma_\mu \gamma_0 \gamma_\nu \gamma_0 = \begin{cases} \gamma_0 & \text{for } \mu = \nu = 0 \\ -\gamma_0 & \text{for } \mu = \nu = i, \end{cases} \quad (3.8)$$

where we only need the case $\mu = \nu$ because the integral [Eq. (3.3)] is otherwise zero. The contribution of this diagram to the flow of u_4 is, therefore,

$$\Delta u_4 = u_4 \frac{8}{N\pi^2} \ln \left[\frac{\Lambda_0}{\Lambda_1} \right] (I_0 - I_1), \quad (3.9)$$

where we have included the factor of 2 coming from an essentially identical diagram where the boson propagator appears connecting the fermion lines on the right instead of on the left. For this specific vertex, the first and third diagrams in Fig. 4 cancel out exactly due to a sign difference in one of the fermion lines. In this particular case, only diagonal flow is generated, i.e., this vertex does not contribute to the flow of the others. In general, however, there is operator mixing: each vertex contributes not only to its own flow but also to other vertices.

Our result turns out to be

$$\begin{aligned} & \mathbf{M}_v(\lambda) \\ &= \frac{8}{N\pi^2} \begin{pmatrix} I_0 + I_1 & -2I_1 & 0 & 0 & 0 & 0 \\ -I_1 & I_0 & 0 & 0 & 0 & 0 \\ 0 & 0 & I_0 - I_1 & 0 & 0 & 0 \\ 0 & 0 & 0 & I_0 - I_1 & 0 & 0 \\ 0 & 0 & 0 & 0 & I_0 & -I_1 \\ 0 & 0 & 0 & 0 & -2I_1 & I_0 + I_1 \end{pmatrix}. \end{aligned} \quad (3.10)$$

B. Wave function renormalization

Upon integration of the high-momentum degrees of freedom, coordinates and fields are defined, which are rescaled versions of the original ones. Doing this explicitly results in the following action:

$$\begin{aligned} S_{\text{eff}} &= - \int dt d^2x' \{ Z_0^{-1} b_1^{-2} \bar{\psi}_a \gamma^0 \partial'_0 \psi_a + Z_1^{-1} b_1^{-1} b_0^{-1} \bar{\psi}_a \gamma^j \partial'_j \psi_a \\ &\quad + \dots \}, \end{aligned} \quad (3.11)$$

where the subscript ‘‘eff’’ indicates that this action describes modes with momenta $|p| < \Lambda_1 = b_1 \Lambda_0$. Here, $t' = b_0 t$, $x' = b_1 x$, $0 < b_0, b_1 < 1$, and \dots contain all the terms in the action, which are not quadratic in the fermion fields. We shall renormalize the field as

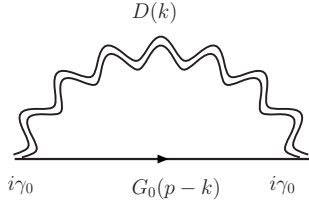


FIG. 5. One-loop self-energy correction to the fermion propagator.

$$\psi_a \rightarrow \psi'_a = Z_0^{-1/2} b_1^{-1} \psi_a \quad (3.12)$$

and enforce the nonrenormalization of the fermion velocity by requiring

$$\frac{Z_1^{-1} b_1^{-1} b_0^{-1}}{Z_0^{-1} b_1^{-2}} = \frac{Z_0 b_1}{Z_1 b_0} = 1, \quad (3.13)$$

which means that the integration shells should actually be nonspherical and have radii related by

$$b_0 = \frac{Z_0}{Z_1} b_1. \quad (3.14)$$

However, $Z_0/Z_1 = 1 + O(1/N)$, therefore the deviation from spherical symmetry is small and is not important to the order of $1/N$ we are considering. Thus, we can compute the loop integral, assuming that the integration region is spherically symmetric.

The one-loop self-energy correction to the inverse fermion propagator was computed in Ref. 4. In our notation, it corresponds to

$$Z_0^{-1} = 1 - \Delta Z_0 = 1 + \frac{4}{N\pi^2} [I_0(\lambda) - I_1(\lambda)] \ln \left[\frac{\Lambda_0}{\Lambda_1} \right], \quad (3.15)$$

$$Z_1^{-1} = 1 - \Delta Z_1 = 1 + \frac{4}{N\pi^2} I_0(\lambda) \ln \left[\frac{\Lambda_0}{\Lambda_1} \right]. \quad (3.16)$$

The correction to the fermion propagator is suppressed by $1/N$, which is another reason to work in the large- N limit. Without this small parameter, the diagram of Fig. 5 would be of order 1.

To see how the wave function renormalization affects the running of the four-Fermi coupling, we write down a generic quartic term in the action

$$u \int dt dx \left(\sum_{a=1}^N \bar{\psi}_a \Gamma \psi_a \right)^2. \quad (3.17)$$

Rescaling of the momenta and the fields as discussed above leads to a renormalization of the coupling constant u according to

$$\begin{aligned} u \rightarrow u' &= b_1^{-2} b_0^{-1} (u + \Delta u) (Z_0^{1/2} b_1^{-1})^{-4} \\ &= b_1 [u + \Delta u + u(\Delta Z_0 + \Delta Z_1)] + O(u^2/N), \end{aligned} \quad (3.18)$$

where we have also included the contribution Δu from the vertex renormalization, and where $\Delta Z_0 + \Delta Z_1$ comes from

wave function renormalization. From Eqs. (3.15) and (3.16), we find

$$\mathbf{M}_{wf}(\lambda) = -\frac{4}{N\pi^2} [2I_0(\lambda) - I_1(\lambda)]. \quad (3.19)$$

IV. RESULTS AND DISCUSSION

Combining Eqs. (3.10) and (3.19), we find

$$\mathbf{M}(\lambda) = \frac{4}{N\pi^2} I_1(\lambda) \begin{pmatrix} 3 & -4 & 0 & 0 & 0 & 0 \\ -2 & 1 & 0 & 0 & 0 & 0 \\ 0 & 0 & -1 & 0 & 0 & 0 \\ 0 & 0 & 0 & -1 & 0 & 0 \\ 0 & 0 & 0 & 0 & 1 & -2 \\ 0 & 0 & 0 & 0 & -4 & 3 \end{pmatrix}. \quad (4.1)$$

Notice that the terms containing $I_0(\lambda)$ cancel out, as anticipated, so that the limit $\lambda \rightarrow \infty$ is finite. The eigenvalues yield the anomalous dimensions: $\gamma_a = \frac{8}{N\pi^2} [5, -1, -1, -1, -1, 5]$. The two operators with the lowest anomalous dimensions, $-40/N\pi^2$, are

$$2(\bar{\psi}_a \psi_a)^2 - (\bar{\psi}_a \gamma_0 \gamma_i \psi_a)^2, \quad 2(\bar{\psi}_a \gamma_5 \psi_a)^2 - (\bar{\psi}_a \gamma_i \psi_a)^2. \quad (4.2)$$

Including the vertices of the form $\gamma^3 \Gamma_j \otimes \gamma^3 \Gamma_j$, which were mentioned in the Introduction, one can repeat the calculation and obtain a copy of the above matrix as a result. This is simply a consequence of $\{\gamma^3, \gamma^\mu\} = 0$. There is no mixing between these new vertices and the ones considered in our calculation. The list of the most relevant operators may then be extended to include

$$2(\bar{\psi}_a \gamma^3 \psi_a)^2 - (\bar{\psi}_a \gamma^3 \gamma_0 \gamma_i \psi_a)^2, \quad 2(\bar{\psi}_a \gamma^3 \gamma_5 \psi_a)^2 - (\bar{\psi}_a \gamma^3 \gamma_i \psi_a)^2, \quad (4.3)$$

whose the anomalous dimensions are also $-40/N\pi^2$.

In the large- N limit, the anomalous dimensions are small; hence, all four-Fermi operators have dimensions close to 4 and are irrelevant. However, as one decreases N , the dimensions of some operators decrease as well. Naively, at

$$N < N_{\text{crit}} = \frac{40}{\pi^2} \approx 4.05, \quad (4.4)$$

the operators in Eqs. (4.2) and (4.3) would have dimensions less than 3 and become relevant. Of course, this is only an extrapolation of our leading-order result to finite N . Nevertheless, it is quite interesting that N_{crit} is close to the real-world value of $N=4$. (For comparison, for the Lorentz-invariant Thirring model, the critical number of four-component Dirac fermions is quoted as 6.6(1),¹⁰ to be compared with $N_{\text{crit}}/2 \approx 2$.) Due to the limitation of our calculations, we cannot determine whether the exact N_{crit} is smaller or larger than 4.

If $N_{\text{crit}} < 4$, then the physics at $N=4$ and infinite coupling is governed by the strong coupling fixed point discussed in

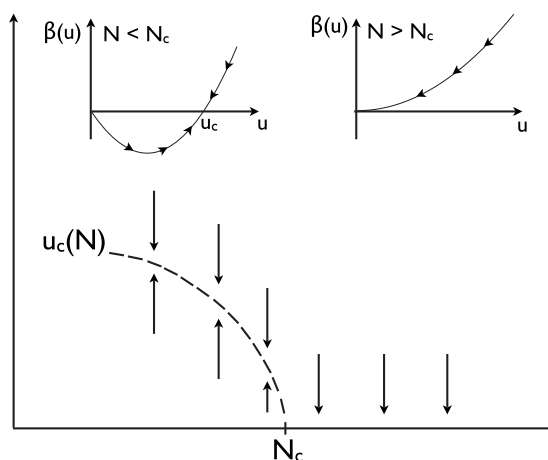


FIG. 6. Phase diagram and beta functions (inset) in one particular scenario.

Ref. 4. If $N_{\text{crit}} > 4$, then there are two further possibilities for $N=4$, $\lambda=\infty$. It may turn out that the system develops a gap and becomes an insulator. In this case, one expects a bifermion operator to have a nonzero expectation value, breaking a discrete symmetry. Unfortunately, simply from the form of the operators in Eqs. (4.2) and (4.3), it is not possible to conclude, with definiteness, which of the discrete symmetries will be spontaneously broken. Another possibility is that the coupling flows into a new stable fixed point (a similar situation was discussed in Ref. 11). In this case, the system remains gapless, but with a dynamic critical behavior. This case is illustrated in Fig. 6, where we also show the β function of the coupling u .

In real graphene, on the other hand, λ is large but not infinite, so in the above discussion, we should take into account that the anomalous dimensions are functions of both N and λ . In real graphene, one has

$$\lambda = \frac{e^2 N}{32 \epsilon_0 \hbar v}, \quad (4.5)$$

where $N=4$ and $v=10^6$ m/s, so that the anomalous dimension of the operators in Eqs. (4.2) and (4.3) is $\gamma \approx -0.72$.

Thus, all four-Fermi operators are irrelevant, at least to the order of $1/N$ we are considering. It is conceivable, however, that higher-order corrections will push γ to be below -1 . On the other hand, for graphene one a SiO_2 substrate with dielectric constant $\epsilon=5.5$, the coupling λ is reduced by a factor of $2/(1+\epsilon)$, and $\gamma \approx -0.45$, substantially above -1 . In this case, one can conclude that the four-Fermi interactions are irrelevant and will become more irrelevant as the fermion velocity v interactions are irrelevant (and will become more irrelevant as the fermion velocity v increases in the infrared).

V. CONCLUSION

We have studied the RG flow of various four-Fermi couplings u in the low-energy theory of graphene, generalized to include N different fermion flavors. We computed the anomalous dimensions of the various couplings to the first nontrivial order in $1/N$. In the limit of infinitely strong Coulomb interaction, the operators with lowest dimensions become relevant for $N < N_{\text{crit}}$, where N_{crit} is estimated to be 4. In real graphene with $N=4$ but at finite Coulomb coupling, the four-Fermi interactions are irrelevant, at least to the leading nontrivial order in $1/N$.

It would be interesting to further investigate the phase diagram of our model. One can try to push the calculations to another order in $1/N$. In addition, one should try to perform numerical simulations of the model. The most interesting values of N where nontrivial phases may exist, as indicated by our calculations, are lower values such as $N=2$ and $N=4$.

Note added. After this work was completed, the authors learned of Ref. 12, in which the running of four-Fermi interactions is also considered. Our lowest anomalous dimension coincides with the value found in Ref. 12, but our values of other anomalous dimensions disagree with Ref. 12. We thank Igor Aleiner for bringing Ref. 12 to our attention.

ACKNOWLEDGMENTS

This work is supported, in part, by DOE under Grant No. DE-FG02-00ER41132.

¹A. K. Geim and K. S. Novoselov, Nat. Mater. **6**, 183 (2007), and references therein.

²G. W. Semenoff, Phys. Rev. Lett. **53**, 2449 (1984).

³J. González, F. Guinea, and M. A. H. Vozmediano, Nucl. Phys. B **424**, 595 (1994).

⁴D. T. Son, Phys. Rev. B **75**, 235423 (2007).

⁵W. Thirring, Ann. Phys. **3**, 91 (1958).

⁶D. Gross and A. Neveu, Phys. Rev. D **10**, 3235 (1974).

⁷E. V. Gorbar, V. P. Gusynin, V. A. Miransky, and I. A. Shovkovy,

Phys. Rev. B **66**, 045108 (2002).

⁸H. Leal and D. V. Khveshchenko, Nucl. Phys. B **687**, 323 (2004).

⁹N. M. R. Peres, F. Guinea, and A. H. Castro Neto, Phys. Rev. B **72**, 174406 (2005).

¹⁰S. Christofi, S. Hands, and C. Strouthos, Phys. Rev. D **75**, 101701(R) (2007).

¹¹I. F. Herbut, Phys. Rev. Lett. **97**, 146401 (2006).

¹²I. L. Aleiner, D. E. Kharzeev, and A. M. Tsvelik, Phys. Rev. B **76**, 195415 (2007).